Deciphering the landscape of host barriers to *Listeria monocytogenes* infection

Ting Zhang[a,b], Sören Abel[a,b,c], Pia Abel zur Wiesch[c,d], Jumpei Sasabe[a,e], Brigid M. Davis[a], Darren E. Higgins[b], and Matthew K. Waldor[a,b,f,1]

[a]Division of Infectious Diseases, Brigham and Women's Hospital, Harvard Medical School, Boston, MA 02115; [b]Department of Microbiology and Immunobiology, Harvard Medical School, Boston, MA 02115; [c]Department of Pharmacy, University of Tromso, The Arctic University of Norway, 9037 Tromso, Norway; [d]Department of Epidemiology of Microbial Diseases, Yale School of Public Health, New Haven, CT 06510; [e]Keio University School of Medicine, Shinjuku-ku, Tokyo 160-8582, Japan; and [f]Howard Hughes Medical Institute, Boston, MA 02115

Edited by Daniel A. Portnoy, University of California, Berkeley, CA, and approved May 4, 2017 (received for review February 24, 2017)

***Listeria monocytogenes* is a common food-borne pathogen that can disseminate from the intestine and infect multiple organs. Here, we used sequence tag-based analysis of microbial populations (STAMP) to investigate *L. monocytogenes* population dynamics during infection. We created a genetically barcoded library of murinized *L. monocytogenes* and then used deep sequencing to track the pathogen's dissemination routes and quantify its founding population (N_b) sizes in different organs. We found that the pathogen disseminates from the gastrointestinal tract to distal sites through multiple independent routes and that N_b sizes vary greatly among tissues, indicative of diverse host barriers to infection. Unexpectedly, comparative analyses of sequence tags revealed that fecally excreted organisms are largely derived from the very small number of *L. monocytogenes* cells that colonize the gallbladder. Immune depletion studies suggest that distinct innate immune cells restrict the pathogen's capacity to establish replicative niches in the spleen and liver. Finally, studies in germ-free mice suggest that the microbiota plays a critical role in the development of the splenic, but not the hepatic, barriers that prevent *L. monocytogenes* from seeding these organs. Collectively, these observations illustrate the potency of the STAMP approach to decipher the impact of host factors on population dynamics of pathogens during infection.**

Listeria monocytogenes | STAMP | pathogen dissemination | pathogen transmission | population dynamics

Some pathogens are able to disseminate from their sites of inoculation to reach distant organs and proliferate to high numbers. During dissemination, pathogens must circumvent host defense mechanisms that restrict access to niches permissive for pathogen replication, which constitute "bottlenecks" constraining pathogen establishment. Understanding pathogen dissemination routes and the extent, timing, and nature of host bottlenecks provides valuable understanding of host–pathogen interactions but can be challenging to investigate experimentally (1). Although dissemination routes and population bottlenecks can, in principle, be determined by meticulous counting of the number of organisms at multiple sites over time, obtaining sufficient spatial and temporal resolution for such studies is often not possible.

Experimental approaches that rely on inoculation of a population of distinguishable, rather than clonal, organisms have been developed to facilitate quantification of population bottlenecks (2–7). Sequence tag-based analysis of microbial populations (STAMP) (8) uses organisms that can be distinguished based on short-sequence barcodes integrated at a neutral position within their genome [also known as wild-type (wt) isogenic tags]. Barcoded organisms from infected animals are enumerated through deep sequencing, and STAMP combines this information with a mathematical framework from classical population genetics to quantify the founding population (N_b) at each infected site (i.e., the number of organisms that survive host bottlenecks and contribute to subsequent population expansion). STAMP enables determination of the N_b with high accuracy and over a wide dynamic range, and the STAMP tags enable assessment of the relatedness among pathogen populations at different sampling sites.

Listeria monocytogenes is a gram-positive, food-borne pathogen that can spread from the gastrointestinal (GI) tract, where it can cause gastroenteritis, to distal sites, including the spleen, liver, gallbladder (GB), brain, and placenta, which can result in meningitis, septic abortion, and other manifestations of systemic infection (9–12). A variety of pathogen factors that enable the organism to grow within host cells and to spread from cell to cell have been identified; additionally, studies of host–pathogen interactions have yielded considerable insight into the host response to *L. monocytogenes* (13–17). However, there is relatively little knowledge of *L. monocytogenes* population dynamics during infection. Portnoy and coworkers (7) and Bakardjiev et al. (10) studied orogastrically infected guinea pigs to identify routes by which *L. monocytogenes* disseminates from the intestine to the liver, mesenteric lymph nodes (MLNs), and spleen, and they have characterized how *L. monocytogenes* traffics between maternal organs and the placenta (7, 10). However, none of these studies measured N_b sizes in these organs.

Here, we used STAMP to map *L. monocytogenes* dissemination routes and quantify N_b sizes following orogastric (OG) and i.v. inoculation of mice. For both infection protocols, we found that N_b size was highest for the liver and spleen, suggesting that a subset of the OG inoculum escapes from the GI tract before constriction of the *L. monocytogenes* N_b there. A markedly lower number of founders gave rise to the *L. monocytogenes* populations in the GB. Unexpectedly, comparative analyses of sequence tags revealed that this organ is the principal source for fecally excreted *L. monocytogenes*. Moreover, using immune depletion and

Significance

Deep sequencing of bar-coded *Listeria monocytogenes* enabled determination of the pathogen's dissemination routes and founding population sizes. The gallbladder, which is seeded by very few *L. monocytogenes* cells, becomes the source for pathogen shedding in the feces. The low complexity of shed populations suggests that genetic drift may be a powerful force in *L. monocytogenes* evolution. Innate immune factors and microbiota differentially regulate pathogen establishment and proliferation at distal sites. Sequence tag-based analysis of microbial populations is a powerful approach for investigating the impact of host factors on pathogen population dynamics.

Author contributions: M.K.W. designed research; T.Z. performed research; T.Z. and D.E.H. contributed new reagents/analytic tools; T.Z., S.A., P.A.z.W., J.S., D.E.H., and M.K.W. analyzed data; and T.Z., S.A., B.M.D., and M.K.W. wrote the paper.

The authors declare no conflict of interest.

This article is a PNAS Direct Submission.

[1]To whom correspondence should be addressed. Email: mwaldor@research.bwh.harvard.edu.

This article contains supporting information online at www.pnas.org/lookup/suppl/doi:10.1073/pnas.1702077114/-/DCSupplemental.

germ-free (GF) mice, we show the potency of the STAMP approach for investigating the impact of host factors on pathogen population dynamics.

Results

***L. monocytogenes* N_b Sizes Vary Among Different Organs.** A library of barcoded but otherwise isogenic *L. monocytogenes* strains was constructed to enable quantitation of the bottlenecks the pathogen confronts within different tissues during infection and to track its dissemination through the body. Each of the strains in the library harbors 1 of 200 unique short (~30 bp) sequence tags inserted into a neutral site (18) on the chromosome. The in vitro growth kinetics of a subset of the tagged strains were indistinguishable from the in vitro growth kinetics of the untagged wt strain (Fig. S1*A*), strongly suggesting that the barcodes do not influence *L. monocytogenes* growth. Based on mathematical modeling, this number of barcodes is sufficient to determine N_b sizes as great as 10^5 with high accuracy (8). Moreover, we experimentally established that we could measure N_b sizes over a wide range with this library using STAMP by comparing the frequencies of tags in an inoculum with the frequencies recovered after exposure to distinct bottlenecks. We plated defined fractions of an in vitro culture of the library (i.e., imposed population bottlenecks) and compared the number of colony-forming units (CFUs) observed on the plates with the calculated number of founders ascertained using STAMP (Fig. S1*B*). There was an excellent correlation between these values ($R^2 = 0.98$) over a range of at least four orders of magnitude (Fig. S1*B*), indicating that this library could be used to estimate bottleneck sizes ranging from as low as three cells to as high as 5×10^5 cells.

The barcoded library was created in *L. monocytogenes* 10403S $InlA^m$, a so-called "murinized" version of a human clinical isolate. This strain expresses a variant of InlA, a surface protein critical for invasion of intestinal epithelial cells, which interacts more efficiently with the murine rather than the human E-cadherin receptor (19). OG inoculation of 10403S $InlA^m$ into adult mice results in a disease that mimics human food-borne listerosis, with dissemination of the pathogen from the GI tract, although large inocula are required (19). Consistent with previous reports, 72 h after BALB/c mice were orogastrically inoculated with the barcoded library (3×10^9 CFUs per mouse), all mice exhibited signs of infection (e.g., ruffled fur, reduced activity) and the pathogen could be isolated from the small intestine (SI), colon, and feces as well as from sites beyond the GI tract, such as the MLNs, liver, spleen, and GB (Fig. 1*A*). *L. monocytogenes* was isolated from the blood and brain as well (Fig. 1*A*), but there was greater variability in the recovery of the pathogen from the latter two tissues than from other sites. The number of CFUs recovered from brain samples was highly correlated with CFU numbers from blood samples ($R^2 = 0.81$), consistent with the model that blood-borne organisms seed the brain.

We enumerated CFUs recovered from each of these sites and estimated the size of the N_b by comparing the frequencies of tags in the inoculum with the frequencies in organisms recovered from the different samples (yielding N_b) and adjusting it with the calibration curve (yielding N_b') (8). In general, similar numbers of *L. monocytogenes* CFUs were recovered from the colon, feces, MLN, spleen, liver, and GB at 3 d postinfection (dpi), with geometric mean values of $\sim 4 \times 10^6$ (Fig. 1*A*), suggesting that these sites all have a fairly similar capacity to carry *L. monocytogenes*. In contrast, N_b' values from these samples displayed more variation (from a mean of 3 in the GB to a mean of 373 in the liver; Fig. 1*A*), suggesting that the magnitude of host restrictions for establishing infection in these locations varies. Unexpectedly, N_b' values were lower in the GI tract [SI (9) and colon (46)] compared with inner organs [spleen (205) and liver (373); $P < 0.01$ for SI vs. spleen or liver, but values for colon vs. spleen or liver did not reach statistical significance; Fig. 1*A*], although the latter sites presumably are colonized by bacteria initially disseminated from the GI tract. The fact that N_b' values for the spleen and liver exceed N_b' values for the GI tract suggests that a subset of the inoculum must have escaped from the GI tract, presumably via the portal vein, lymphatics, or systemic circulation (7), before restriction of the population there. The N_b' values for the SI at 3 dpi predominantly reflect intracellular *L. monocytogenes* because they were similar for tissue treated with gentamicin, which kills extracellular organisms, and untreated SI tissues (Fig. 1*A*). The fact that even the largest calculated N_b' values were at least six orders of magnitude lower than the inoculum size of 3×10^9 CFUs per mouse indicates that there is an extremely severe bottleneck for *L. monocytogenes* to establish infection in this model; the different N_b sizes in the tested host tissues reveal that additional tissue-specific bottlenecks constrain the capacity of *L. monocytogenes* to access different host organs.

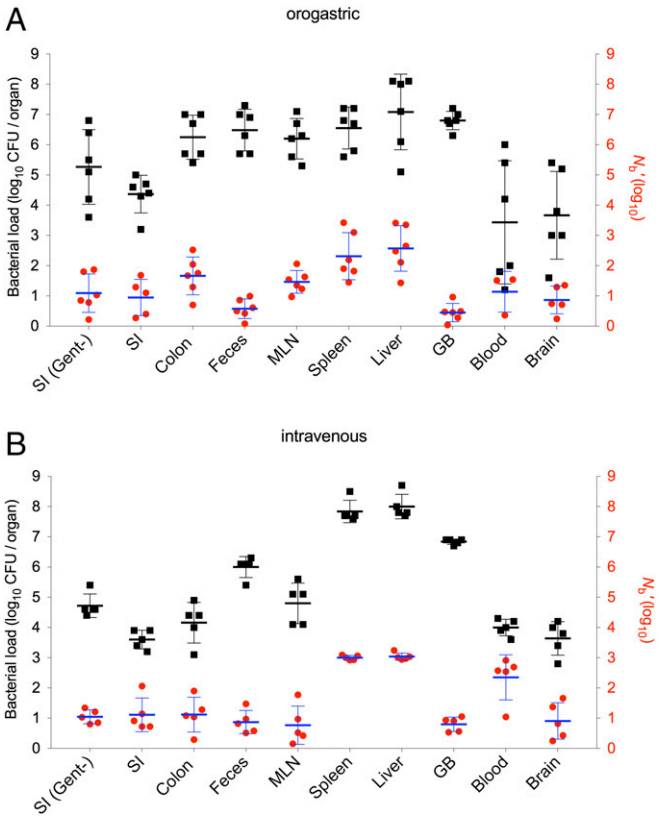

Fig. 1. Recovered CFU and N_b' sizes in different tissues following OG or i.v. inoculation of *L. monocytogenes*. BALB/c mice were orogastrically inoculated with 3×10^9 CFUs of *L. monocytogenes* (10403S $InlA^m$) (*A*) or injected i.v. with 6×10^4 CFUs (*B*). Bacterial loads (CFU, black squares) and N_b sizes (N_b', red circles) in different tissues were determined 3 d after OG infection or 2 d after i.v. infection. CFU values are expressed per organ for the SI, colon, MLN, spleen, liver, GB, and brain; they are expressed per milliliter for blood and per pellet for feces. Each black square and red circle represents data from one mouse. Geometric means (horizontal lines) and SD (whiskers) are shown. SI (Gent–), gentamicin-negative (untreated SI tissues).

The lowest N_b' values were found in the GB. Even though there was $N_b' \leq 9$ in the GB samples (mean $N_b' = 3$, N_b' range: 1–9), the numbers of *L. monocytogenes* CFUs recovered from these samples were comparable to the numbers found in other tissues (Fig. 1*A*). Thus, host barriers appear to restrict access of *L. monocytogenes* to the GB severely; however, once the pathogen reaches this site, presumably by passing through the hepatic duct and then ascending through the cystic duct, it is capable of replicating to high densities. The GB is known to be relatively deficient in its capacity to recruit innate immune effector cells

MICROBIOLOGY

such as neutrophils (20), likely accounting for the high density of organisms found there. Notably, despite the relatively large N_b' value observed in the colon (mean = 46), the N_b' value in the feces was very low and similar to the N_b' value in the GB, suggesting that fecal organisms are not principally derived from intracellular organisms replicating within colonic tissue.

Historically, many studies have used i.v. inoculation of *L. monocytogenes* as a model to investigate in vivo pathogen–host interactions. In contrast to OG inoculation, the i.v. route introduces a high number of bacteria into the blood at the same time. It bypasses gut barriers that may prevent *L. monocytogenes* dissemination, and the pathogen can directly seed the spleen and liver. We measured N_b' and CFU values 2 d after i.v. inoculation of 6×10^4 CFUs. At this dose and time, the mice exhibit similar signs of disease observed 3 d after OG inoculation. Although N_b' and CFU values were generally similar for i.v. and OG inoculation (Fig. 1 *A* vs. *B*), there were some differences dependent upon the route of inoculation. For example, N_b' values tended to be higher and less varied in the spleen and liver after i.v. vs. OG inoculation, consistent with the pathogen's direct and immediate access to these organs after i.v. inoculation. Not surprisingly, N_b' values were also higher in blood after i.v. injection compared with OG inoculation, and CFU counts had a lower variance. Similarly, CFU counts recovered from brain samples also exhibited lower variance with the i.v. infection route, consistent with hematogenous seeding of the brain. The i.v. infection route did not increase the particularly low N_b' values that were observed in fecal, GB, and brain samples with OG inoculation, suggesting that escape from the intestine is not the primary impediment to colonization of these sites (Fig. 1 *A* and *B*).

The GB Is the Reservoir for Fecal Shedding of *L. monocytogenes*. Besides enabling calculation of N_b sizes, the sequence tags facilitate comparisons of the genetic relatedness among populations from different samples, which can be calculated by comparing tag frequencies within populations. The most striking finding from these analyses was the high degree of genetic relatedness between populations resident in the GB and the feces after either OG (3 dpi) or i.v. inoculation, which was far higher than the relatedness of GB or fecal populations to populations from any other tissue (Fig. 2 *A* and *B*, respectively, and Fig. S2 *A*–*C*). Animals were often found to contain the same single predominant tagged strain in samples from both sites (consistent with the low N_b' values for these sites); however, the identity of this tag differed among mice, indicating that a selective advantage does not account for a particular strain's predominance within GB and fecal samples (Fig. 2*C*). Notably, there was far less correspondence between fecal populations and populations within colonic tissue, and colonic samples were typically not dominated by a single tagged strain (Fig. 2*C*). Collectively, these data provide further support for the idea that *L. monocytogenes* replicating intracellularly within colonic tissue is not the predominant source of the pathogen shed in feces; instead, the GB serves as the reservoir for bacteria likely to be fecally transmitted. The similarity between the populations in the GB and feces was not as marked 2 d after OG inoculation, likely because some of the fecal bacteria are still derived from the inoculum (Fig. 2*A* and Fig. S3).

Additional pairwise comparisons between *L. monocytogenes* populations in samples from different sites showed that the genetic relatedness between samples from different sites was generally low for animals inoculated by the OG route (Fig. S2*A*). This finding suggests that *L. monocytogenes* may arrive at sites distal to the GI tract through multiple independent paths, rather than seeding a primary niche from which bacteria subsequently spread. These observations are consistent with episodic spread of the population from the OG inoculum through the portal vein, and perhaps other routes, to the liver and via lymphatics and systemic circulation to the MLN and spleen as proposed by Melton-Witt et al. (7). In contrast, after i.v. inoculation, the

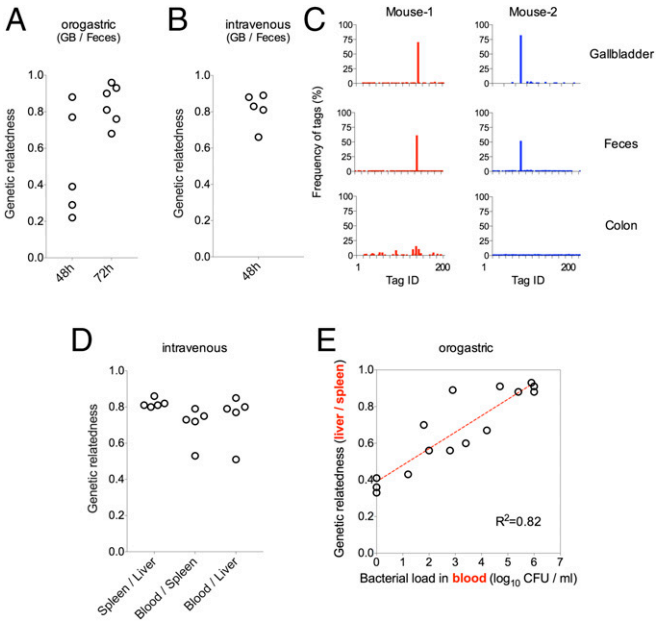

Fig. 2. Genetic relatedness of *L. monocytogenes* populations isolated from different tissues. Genetic relatedness of *L. monocytogenes* populations in the indicated samples 48 h and/or 72 h after OG inoculation (*A*) and 48 h after i.v. inoculation (*B* and *D*). (*C*) Relative frequencies of barcodes in the GB, feces, and colon of two representative mice. (*E*) Correlation between the *L. monocytogenes* burden in the blood (*x* axis) and the genetic relatedness of *L. monocytogenes* populations in the spleen and liver (*y* axis) 48 and 72 h after OG inoculation of mice. The Pearson correlation coefficient value was used to quantify correlation. Each open circle in *A*, *B*, *D*, and *E* represents data from one mouse.

L. monocytogenes recovered from blood, spleen, and liver samples were all closely related (Fig. 2*D*), consistent with bacterial injection into the bloodstream and subsequent filtration and sequestration by the spleen and liver. In animals inoculated by the OG route, bacterial populations in the liver and spleen tended to become more related as the bacterial load in the blood increased (Fig. 2*E*). However, in the absence of high-grade bacteremia (bacterial load < 1,000 CFU/mL; Fig. 2*E*), the samples' relative lack of relatedness suggests that they are seeded by independent processes. These findings suggest a model in which the liver and spleen are seeded with distinct founders at an early stage of the infection; subsequently, as the pathogen burden increases, the blood enables exchange of bacteria between the two organs. Furthermore, following OG inoculation, it is likely that pathogen arrival at the liver and spleen is progressive, because N_b' values tended to increase from day 2 to day 3 following inoculation (Fig. 1*A* vs. Fig. S3).

We investigated whether *L. monocytogenes* chemotaxis and/or motility modulates the pathogen's capacity to reach or proliferate within colonized sites by performing infections with a Δ*cheA* *L. monocytogenes* strain, which is defective in both chemotaxis and motility (Fig. 3*A*). Following OG inoculation of mice with the barcoded Δ*cheA* mutant, N_b and CFU values from the spleen, liver, and GB samples were very similar to the values obtained with inoculation of the wt strain (Fig. 1*A* vs. 3*B*). Furthermore, when the barcoded Δ*cheA* and wt libraries were coinoculated orogastrically, the Δ*cheA* mutant was found to have a competitive index of ~1 relative to the wt strain (i.e., no colonization deficit) (Fig. 3*C*), and Δ*cheA* and wt strains were equally likely to be the dominant strain isolated from GB samples (Fig. 3*D*). Together, these observations all suggest that neither chemotaxis nor motility modulates the capacity of *L. monocytogenes* to reach or colonize the GB, liver, spleen, and MLN.

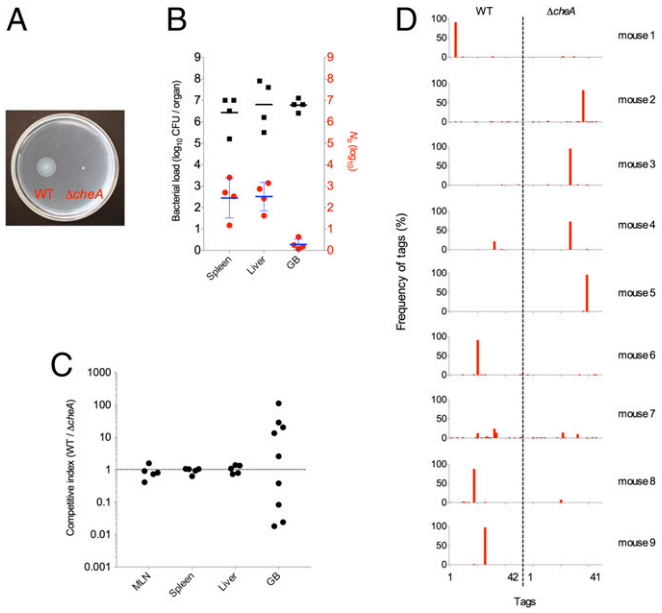

Fig. 3. Chemotaxis and motility are not required for *L. monocytogenes* to breach intestinal barriers and reach distal infection sites. (*A*) Motility of wt (WT) and Δ*cheA L. monocytogenes* in 0.3% agar plates. (*B*) CFU and N_b sizes for the indicated tissues at 3 dpi of mice inoculated orogastrically with 3×10^9 CFUs of Δ*cheA L. monocytogenes*. Each black square and red circle represents data from one mouse. Geometric means (horizontal lines) and SD (whiskers) are shown. (*C*) Competitive indexes for the indicated tissues from mice inoculated orogastrically with a 1:1 mixture of barcoded Δ*cheA* and wt *L. monocytogenes*. Each black circle represents data from one mouse. (*D*) Relative frequencies of *L. monocytogenes* barcodes in the GB of infected mice; data are from two litters of mice (n = 9) that were infected on different days.

Different Host Innate Immune Factors Contribute to Restricting *L. monocytogenes* N_b Sizes in the Spleen and Liver. To begin to explore the host factors that control *L. monocytogenes* N_b sizes in various tissues, we treated mice with antibodies against components of the innate immune response before inoculation of the pathogen. Inoculation via the i.v. route, which is known to deliver an initial synchronous bolus of the pathogen to the liver (~80% of inoculum) and spleen (~20% of inoculum) (21), was used for these experiments because this infection route has been used for similar immune depletion studies in the past (22). Prior studies have established that after i.v. inoculation, there are two stages of *L. monocytogenes* growth in the spleen and liver: a lag phase (first 6 h), followed by an exponential expansion phase (21). During the lag phase, there is no net proliferation of the pathogen in the spleen, whereas in the liver, there is a net reduction in the *L. monocytogenes* cells during this stage (23). Most (~80%) of the *L. monocytogenes* cells that reach the liver are thought to be captured and subsequently inactivated by Kupffer cells during the lag phase, whereas the remaining *L. monocytogenes* cells enter hepatocytes, where they can replicate (23–25).

Mice were treated with an antibody to Gr-1, which is expressed on myelomonocytic cells (MMCs), including neutrophils and monocytes, at doses known to deplete cells bearing this marker (26). This treatment leads to an accelerated course of disease (22); therefore, tissue samples for analyses were obtained 24 h after infection. Consistent with previous reports, more *L. monocytogenes* CFUs were recovered from the spleen and liver (22), as well as from the GB of anti–Gr-1–treated mice, than from control animals (Fig. 4*A*). The N_b' values were also elevated in the spleen and GB (Fig. 4*A*), suggesting that Gr-1–bearing cells (or some process that requires these cells) restrict the size of the N_b' in these two organs and likely restrain the pathogen's subsequent replication in these sites as well. In the spleen, N_b' values in anti–Gr-1–treated animals were elevated to values that are close to the predicted fraction of the inoculum initially captured by this organ (~20% of the inoculum), suggesting that the anti–Gr-1 treatment ablated the spleen's capacity to hinder *L. monocytogenes* in establishing a replicative niche. In contrast, N_b' values in the livers of control and anti–Gr-1–treated mice did not differ, even though ~60-fold more *L. monocytogenes* CFUs were recovered from the livers of treated mice (Fig. 4*A*). This discrepancy suggests that MMCs do not play a major role in modulating *L. monocytogenes*' initial access to and establishment within hepatocytes, but that these cells restrict the subsequent expansion of the *L. monocytogenes* population, perhaps by killing *L. monocytogenes* released from lysed hepatocytes during the later stage of *L. monocytogenes* proliferation (21, 23).

Mice were also treated with antibody to TNF-α, a cytokine that promotes the activity of macrophages (including Kupffer cells in the liver), monocytes, and neutrophils (27–29). For these experiments, tissue samples were collected 2 d after i.v. inoculation of *L. monocytogenes*. Similar to anti–Gr-1–treated mice, the numbers of *L. monocytogenes* CFUs recovered from the spleens and livers of anti–TNF-α–treated mice were elevated compared with control animals (Fig. 4*B*). However, in contrast to anti–Gr-1 treatment, administration of antibody to TNF-α elevated N_b' values in the livers, but not in the spleens, of treated mice (Fig. 4*B*). The elevation of hepatic N_b' values in response to TNF-α inactivation, but not in response to anti–Gr-1 treatment, which depletes monocytes and neutrophils, suggests that the pathogen's capacity to establish infection in the liver may be restricted by Kupffer cells. These cells are known to produce antimicrobial products (e.g., reactive oxygen species, superoxide) in response to TNF-α stimulation (30), and their activity is reduced by anti–TNF-α treatment (30). Taken together, the observations from the antibody depletion experiments suggest that different innate immune cell types restrict the capacity of *L. monocytogenes* to establish infection in the spleen and liver.

In addition to its effect on liver and spleen colonization, pretreatment with anti–TNF-α mAb significantly increased the N_b' values for GBs (Fig. 4*B*) of mice inoculated i.v. with *L. monocytogenes*. However, inactivation of TNF-α did not change the bacterial burden in the GB (Fig. 4*B*), suggesting that TNF-α activity restricts the capacity of *L. monocytogenes* to access/establish in this organ but not its subsequent proliferation to 10^7 CFUs,

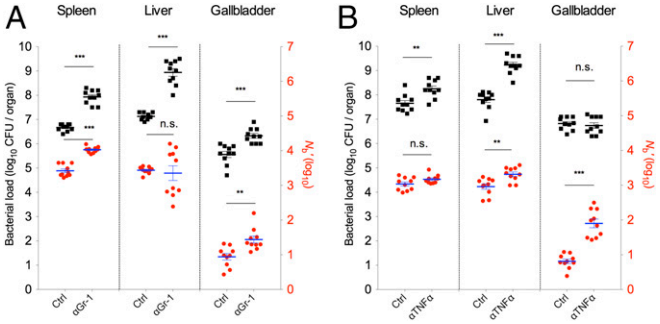

Fig. 4. Modulation of the capacity of *L. monocytogenes* to establish and proliferate in the spleen, liver, and GB following treatment with monoclonal anti–Gr-1 or anti–TNF-α antibodies. Control (Ctrl) and anti–Gr-1 mAb-treated mice (*A*) or anti–TNF-α–treated mice (*B*) were infected i.v. with 6×10^4 CFUs of *L. monocytogenes*. CFU (black squares) and N_b' (red circles) values for the indicated tissues were determined 1 dpi in the anti–Gr-1–treated mice and 2 dpi in the anti–TNF-α–treated mice. The data are from two litters of mice (n = 10) that were infected on different days. Each black square and red circle represents data from one mouse. Geometric means (horizontal lines) and SEM (whiskers) are shown. The Mann–Whitney test was used to assess significance: $*P < 0.05$, $**P < 0.01$, $***P < 0.001$. n.s., no significance.

which may represent the maximal carrying capacity of the GB for *L. monocytogenes*.

Microbiota Augments Splenic but Not Hepatic Barriers to the Pathogen. The intestinal microbiota can play a direct role in protecting the host from intestinal pathogens (31). In addition, the microbiota exerts indirect yet critical influences on pathogen–host interactions by modulating the development of several host organ systems, including the innate and adaptive immune systems (32). We compared *L. monocytogenes* CFU and N_b' values from the spleen, liver, and GB from conventional [specific pathogen-free (SPF)] and GF Swiss Webster mice following i.v. inoculation of the pathogen. Elevated CFUs were recovered from the spleens and livers of GF mice relative to SPF mice, as observed previously in C57BL/6 mice (33), but no increase was observed in CFUs recovered from the GB (Fig. 5*A*). The elevated *L. monocytogenes* CFU values in spleens from GF mice were accompanied by elevated N_b' values in this tissue (Fig. 5*A*), whereas hepatic GF samples only showed an increase in CFUs. Thus, the alterations seen in GF livers and spleens parallel the alterations observed in anti–Gr-1–treated animals (compare Figs. 4*A* and 5*A*), raising the possibility that the absence of microbiota impairs development of neutrophils and/or monocytes that are targeted by the anti–Gr-1 treatment. Depletion of gut microbiota by oral administration of broad-spectrum antibiotics for 17 d, which resulted in a 2×10^5-fold reduction in amplifiable 16S rRNA sequences in feces, did not alter splenic or hepatic bacterial loads or N_b' values (Fig. 5*B*), consistent with reports that the microbiota must be present during an early critical period to shape innate immune development (34). Previous studies have suggested that the intestinal microbiota enhances the bactericidal activity of bone marrow-derived neutrophils (35) and promotes the differentiation of granulocyte and monocyte progenitors in the bone marrow and spleen (33), which might underlie the distinct CFU and N_b' values we observed for spleens of GF and SPF animals. However, the similarity of N_b' values in livers from GF and SPF mice suggests that the gut microbiota does not markedly shape the capacity of Kupffer cells or any other hepatic innate immune cells that restrict the establishment of *L. monocytogenes* in the liver. Taken together, our experiments suggest that the microbiota exerts distinct roles in the development of splenic and hepatic innate immune cells.

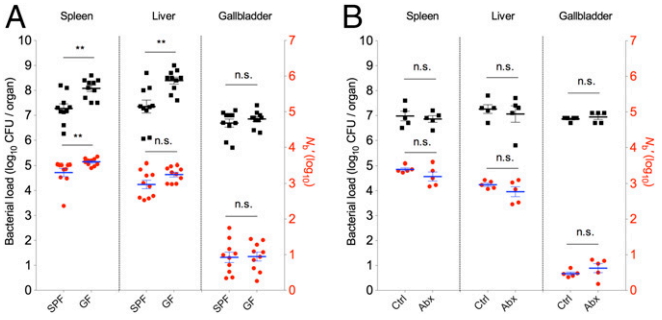

Fig. 5. Modulation of host barriers to *L. monocytogenes* infection by the microbiota. (*A*) GF and SPF Swiss Webster mice were inoculated i.v. with 6×10^4 *L. monocytogenes* CFUs. CFU (black squares) and N_b' (red circles) values in the indicated tissues were determined 2 d later. Data are from two litters of mice ($n = 10$) that were infected on different days. Each black square and red circle represents data from one mouse. (*B*) Antibiotic-treated (Abx) Swiss Webster mice and nontreated control mice were inoculated i.v. with 6×10^4 *L. monocytogenes* CFUs. CFU (black squares) and N_b' (red circles) values in the indicated tissues were determined 2 d later. Each black square and red circle represents data from one mouse. Geometric means (horizontal lines) and SEM or SD (whiskers, *A* and *B*, respectively) are shown. The Mann–Whitney test was used to assess significance: $*P < 0.05$, $**P < 0.01$, $***P < 0.001$.

Discussion

We took advantage of STAMP, using barcoded but otherwise isogenic *L. monocytogenes*, to quantify the effects of host barriers on this food-borne pathogen's capacity to establish a replicative niche (i.e., defined N_b) in various host organs following OG or i.v. inoculation. We found that *L. monocytogenes* populations with distinct composition and complexity arise within the spleen, liver, GB, and other tissues due to organ-specific restrictions imposed by innate immune factors and the microbiota, as well as by the existence of multiple dissemination pathways (Fig. S4). The i.v. infection route did not increase the particularly low N_b' values that were observed in fecal, GB, and brain samples with OG inoculation, suggesting that escape from the intestine is not the primary barrier to colonization of these sites. Surprisingly, N_b' values in the SI and colon were similar regardless of the route of inoculation. Thus, the number of niches available for *L. monocytogenes* replication in intestinal tissue does not appear to be primarily determined by the route (intestinal tract vs. blood) through which the pathogen reaches these sites. Collectively, our observations illustrate the power of the STAMP approach to decipher the impact of host factors on population dynamics of pathogens during infection.

Besides enabling quantification of N_b sizes, STAMP facilitates comparative analyses of the genetic diversity of populations recovered from different host organs. Prior studies by Contag and coworkers (12) revealed that the GB is routinely colonized in mice infected with *L. monocytogenes*, but did not discern the full ramifications of this finding. Here, by comparing the barcodes of *L. monocytogenes* recovered from the GB and feces, we discovered that the GB is the principal source for *L. monocytogenes* shed in the feces. Organisms recovered from the GB and feces usually contained the same single highly dominant tag, although the identity of the tag differed among animals. Although fecal-oral transmission is not an important route of *L. monocytogenes* transmission in humans, it is thought to be important in ruminants in the wild (36). Thus, if the GBs of ruminant animals are colonized with *L. monocytogenes* in a pauciclonal manner as we have observed in mice, then it is likely that pauciclonal fecal-oral transmission of *L. monocytogenes* occurs in the wild. With such a restrictive bottleneck limiting transmission of the pathogen, it is likely that genetic drift is a potent force in shaping *L. monocytogenes* evolution in the wild. Furthermore, our findings suggest an unexpected similarity between *L. monocytogenes* and *Salmonella enterica* serotype Typhi, for which the GB is the reservoir for *S. typhi* transmitted among humans (37).

Both MMCs and TNF-responsive cells limit the capacity of *L. monocytogenes* to establish a replicative niche in the GB; however, additional studies are required to define host and pathogen factors further that account for the profound restriction of the *L. monocytogenes* N_b size in this organ. We speculate that a very small pauciclonal *L. monocytogenes* population seeds the GB early in infection and that this population receives unfettered access to niches in which rapid replication is possible. This initial N_b' value may be derived from the first pathogen cells to lyse out of infected hepatocytes and migrate through the bile to the GB. Subsequently, after the initial replication of these founders, resources for replication of "late arrivers" to the GB are restricted and they are at a competitive disadvantage. This scenario, which is similar to the "priority effect" proposed by Lam and Monack (5) to explain the clonality of *Salmonella enterica* serovar *Typhimurium* observed during chronic colonization of the murine colon, assumes that there are a relatively finite number of niches optimal for *L. monocytogenes* replication in the GB. It is also possible that the growth of the *L. monocytogenes* founders in the GB induces expression of pathogen factors that antagonize growth of the late arrivers. Further studies to elucidate the molecular mechanisms that account for the highly restricted size of the founding *L. monocytogenes* population in the GB are warranted. Indeed,

deeper understanding of the *L. monocytogenes* factors that facilitate its replication in the GB could contribute to the creation of safer live-attenuated *L. monocytogenes* strains for use as vaccine vectors and in cancer therapeutics (38).

Materials and Methods

The STAMP protocol used here was similar to the STAMP protocol described by Abel et al. (8). For most in vivo studies, 8-wk-old female BALB/c mice were orogastrically inoculated with 3×10^9 CFUs of barcoded *L. monocytogenes* 10403S InlA^m; 48 h and 72 h after inoculation, animals were euthanized and organs (proximal SI, colon, MLN, spleen, liver, GB, blood, and brain), as well as fecal pellets, were collected and homogenized. All of the homogenates/samples were plated on BHI-streptomycin plates for CFU enumeration and N_b analysis. For N_b analysis, *L. monocytogenes* colonies were washed off plates, genomic DNA was extracted, and the region harboring the 30-bp barcodes was amplified using primer PLM30 and primer PLM6-P29 (Table S1). The purified PCR products were combined in equimolar concentrations and sequenced on an Illumina MiSeq machine using primer PLM49. Reaper-12–340 was used to discard sequence reads with low quality (≤Q30) and trim the sequence following the barcode. The trimmed sequences were clustered with QIIME (version 1.6.0) using pick_otus.py with a sequence similarity threshold of 0.9. Then, N_b was calculated and adjusted by the calibration curve to yield N_b' using an R script (8). Genetic distance was estimated using the Cavalli–Sforza chord distance method (39) as described by Abel et al. (8). Genetic relatedness is 1 − genetic distance. The animal protocol used for this study was reviewed and approved by Harvard Medical Area Standing Committee on Animals. All methods are described in detail in *SI Materials and Methods*.

ACKNOWLEDGMENTS. We thank members of the M.K.W. laboratory for helpful discussion. This work is supported by NIH Grant R37-AI-042347 (to M.K.W.), the Howard Hughes Medical Institute (M.K.W.), Research Council of Norway (NFR) Grant 249979 (to S.A.), and Helse-Nord Grant 14796 (to S.A.).

1. Abel S, Abel zur Wiesch P, Davis BM, Waldor MK (2015) Analysis of bottlenecks in experimental models of infection. *PLoS Pathog* 11:e1004823.
2. Barnes PD, Bergman MA, Mecsas J, Isberg RR (2006) Yersinia pseudotuberculosis disseminates directly from a replicating bacterial pool in the intestine. *J Exp Med* 203: 1591–1601.
3. Grant AJ, et al. (2008) Modelling within-host spatiotemporal dynamics of invasive bacterial disease. *PLoS Biol* 6:e74.
4. Kaiser P, Slack E, Grant AJ, Hardt WD, Regoes RR (2013) Lymph node colonization dynamics after oral Salmonella Typhimurium infection in mice. *PLoS Pathog* 9: e1003532.
5. Lam LH, Monack DM (2014) Intraspecies competition for niches in the distal gut dictate transmission during persistent Salmonella infection. *PLoS Pathog* 10:e1004527.
6. Lim CH, et al. (2014) Independent bottlenecks characterize colonization of systemic compartments and gut lymphoid tissue by Salmonella. *PLoS Pathog* 10:e1004270.
7. Melton-Witt JA, Rafelski SM, Portnoy DA, Bakardjiev AI (2012) Oral infection with signature-tagged Listeria monocytogenes reveals organ-specific growth and dissemination routes in guinea pigs. *Infect Immun* 80:720–732.
8. Abel S, et al. (2015) Sequence tag-based analysis of microbial population dynamics. *Nat Methods* 12:223–226.
9. Lecuit M, et al. (2001) A transgenic model for listeriosis: Role of internalin in crossing the intestinal barrier. *Science* 292:1722–1725.
10. Bakardjiev AI, Theriot JA, Portnoy DA (2006) Listeria monocytogenes traffics from maternal organs to the placenta and back. *PLoS Pathog* 2:e66.
11. Disson O, Lecuit M (2012) Targeting of the central nervous system by Listeria monocytogenes. *Virulence* 3:213–221.
12. Hardy J, et al. (2004) Extracellular replication of Listeria monocytogenes in the murine gall bladder. *Science* 303:851–853.
13. Disson O, Lecuit M (2013) In vitro and in vivo models to study human listeriosis: Mind the gap. *Microbes Infect* 15:971–980.
14. Portnoy DA, Auerbuch V, Glomski IJ (2002) The cell biology of Listeria monocytogenes infection: The intersection of bacterial pathogenesis and cell-mediated immunity. *J Cell Biol* 158:409–414.
15. Agaisse H, et al. (2005) Genome-wide RNAi screen for host factors required for intracellular bacterial infection. *Science* 309:1248–1251.
16. Cossart P (2011) Illuminating the landscape of host-pathogen interactions with the bacterium Listeria monocytogenes. *Proc Natl Acad Sci USA* 108:19484–19491.
17. Witte CE, et al. (2012) Innate immune pathways triggered by Listeria monocytogenes and their role in the induction of cell-mediated immunity. *Adv Immunol* 113:135–156.
18. Lauer P, Chow MY, Loessner MJ, Portnoy DA, Calendar R (2002) Construction, characterization, and use of two Listeria monocytogenes site-specific phage integration vectors. *J Bacteriol* 184:4177–4186.
19. Wollert T, et al. (2007) Extending the host range of Listeria monocytogenes by rational protein design. *Cell* 129:891–902.
20. Gonzalez-Escobedo G, Gunn JS (2013) Gallbladder epithelium as a niche for chronic Salmonella carriage. *Infect Immun* 81:2920–2930.
21. Conlan JW (1999) Early host-pathogen interactions in the liver and spleen during systemic murine listeriosis: An overview. *Immunobiology* 201:178–187.
22. Carr KD, et al. (2011) Specific depletion reveals a novel role for neutrophil-mediated protection in the liver during Listeria monocytogenes infection. *Eur J Immunol* 41: 2666–2676.
23. Gregory SH, Sagnimeni AJ, Wing EJ (1996) Bacteria in the bloodstream are trapped in the liver and killed by immigrating neutrophils. *J Immunol* 157:2514–2520.
24. Broadley SP, et al. (2016) Dual-track clearance of circulating bacteria balances rapid restoration of blood sterility with induction of adaptive immunity. *Cell Host Microbe* 20:36–48.
25. Zeng Z, et al. (2016) CRIg functions as a macrophage pattern recognition receptor to directly bind and capture blood-borne gram-positive bacteria. *Cell Host Microbe* 20: 99–106.
26. Waite JC, et al. (2011) Dynamic imaging of the effector immune response to listeria infection in vivo. *PLoS Pathog* 7:e1001326.
27. Roca FJ, Ramakrishnan L (2013) TNF dually mediates resistance and susceptibility to mycobacteria via mitochondrial reactive oxygen species. *Cell* 153:521–534.
28. Xiong H, et al. (2016) Innate lymphocyte/Ly6C(hi) monocyte crosstalk promotes Klebsiella pneumoniae clearance. *Cell* 165:679–689.
29. Kolaczkowska E, Kubes P (2013) Neutrophil recruitment and function in health and inflammation. *Nat Rev Immunol* 13:159–175.
30. Nakashima H, et al. (2008) Superoxide produced by Kupffer cells is an essential effector in concanavalin A-induced hepatitis in mice. *Hepatology* 48:1979–1988.
31. Caballero S, Pamer EG (2015) Microbiota-mediated inflammation and antimicrobial defense in the intestine. *Annu Rev Immunol* 33:227–256.
32. Honda K, Littman DR (2016) The microbiota in adaptive immune homeostasis and disease. *Nature* 535:75–84.
33. Khosravi A, et al. (2014) Gut microbiota promote hematopoiesis to control bacterial infection. *Cell Host Microbe* 15:374–381.
34. Gensollen T, Iyer SS, Kasper DL, Blumberg RS (2016) How colonization by microbiota in early life shapes the immune system. *Science* 352:539–544.
35. Clarke TB, et al. (2010) Recognition of peptidoglycan from the microbiota by Nod1 enhances systemic innate immunity. *Nat Med* 16:228–231.
36. Nightingale KK, et al. (2004) Ecology and transmission of Listeria monocytogenes infecting ruminants and in the farm environment. *Appl Environ Microbiol* 70: 4458–4467.
37. Gunn JS, et al. (2014) Salmonella chronic carriage: Epidemiology, diagnosis, and gallbladder persistence. *Trends Microbiol* 22:648–655.
38. Le DT, et al. (2015) Safety and survival with GVAX pancreas prime and Listeria Monocytogenes-expressing mesothelin (CRS-207) boost vaccines for metastatic pancreatic cancer. *J Clin Oncol* 33:1325–1333.
39. Cavalli-Sforza LL, Edwards AW (1967) Phylogenetic analysis. Models and estimation procedures. *Am J Hum Genet* 19:233–257.
40. Whiteley AT, Pollock AJ, Portnoy DA (2015) The PAMP c-di-AMP is essential for Listeria monocytogenes growth in rich but not minimal media due to a toxic increase in (p)ppGpp. *Cell Host Microbe* 17:788–798.
41. Disson O, et al. (2009) Modeling human listeriosis in natural and genetically engineered animals. *Nat Protoc* 4:799–810.
42. Mead R (1988) *The Design of Experiments* (Cambridge Univ Press, Cambridge, UK).
43. Reikvam DH, et al. (2011) Depletion of murine intestinal microbiota: Effects on gut mucosa and epithelial gene expression. *PLoS One* 6:e17996.